Inorganic Chemistry

Article

pubs.acs.org/IC

Platinum-Modified Adenines: Unprecedented Protonation Behavior Revealed by NMR Spectroscopy and Relativistic Density-Functional Theory Calculations†

Jan Vícha, Gabriel Demo, and Radek Marek*

National Center for Biomolecular Research, Faculty of Science and Central European Institute of Technology-CEITEC, Masaryk University, Kamenice 5/A4, CZ-62500 Brno, Czech Republic

Supporting Information

ABSTRACT: Two novel Pt^{IV} complexes of aromatic cytokinins with possible antitumor properties were prepared by reaction of selected aminopurines with K_2PtCl_6. The structures of both complexes, 9-[6-(benzylamino)purine] pentachloroplatinate (IV) and 9-[6-(furfurylamino)purine] pentachloroplatinate (IV), were characterized in detail by using two-dimensional NMR spectroscopy (^1H, ^{13}C, ^{15}N, and ^{195}Pt) in solution and CP/MAS NMR techniques in the solid state. We report for the first time the X-ray structure of a nucleobase adenine derivative coordinated to Pt^{IV} via the N9 atom. The protonation equilibria for the complexes in solution were characterized by using NMR spectroscopy (isotropic chemical shifts and indirect nuclear spin−spin coupling constants) and the structural conclusions drawn from the NMR analysis are supported by relativistic density-functional theory (DFT) calculations. Because of the presence of the Pt atom, hybrid GGA functionals and scalar-relativistic and spin−orbit corrections were employed for both the DFT calculations of the molecular structure and particularly for the NMR chemical shifts. In particular, the populations of the N7-protonated and neutral forms of the complexes in solution were characterized by correlating the experimental and the DFT-calculated NMR chemical shifts. In contrast to the chemical exchange process involving the N7−H group, the hydrogen atom at N3 was determined to be unexpectedly rigid, probably because of the presence of the stabilizing intramolecular interaction N3−H···Cl. The described methodology combining the NMR spectroscopy and relativistic DFT calculations can be employed for characterizing the tautomeric and protonation equilibria in a large family of transition-metal-modified purine bases.

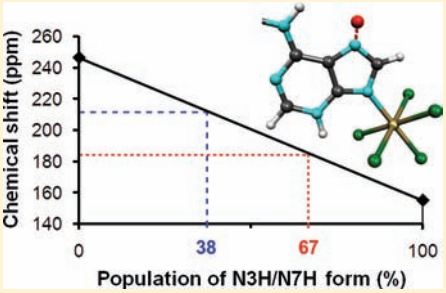

1. INTRODUCTION

Since the discovery of cisplatin in the 1960s,[1] great efforts have been expended on the preparation of various transition-metal complexes with potential antitumor activity. The main goal of these investigations was to suppress the negative effects of cisplatin (e.g., neurotoxicity, nephrotoxicity, nausea).[2] A myriad of new Pt^{II} complexes have been prepared and characterized.[3−5] The search for complexes with potential antitumor activity soon broadened the field to include various transition metals which can serve as Pt^{II} substitutes. Pd^{II} complexes are very important analogs of Pt^{II} complexes, with several examples showing very promising properties.[6,7] However, one should keep in mind that Pt shows strong antitumor effects not only in oxidation state II. Similar properties have been reported for Pt^{IV} complexes.[8] Their anticancer activity has been known for a long time,[9] but they have been studied less extensively than their Pt^{II} analogs. However, a recent renaissance of Pt^{IV} investigations has been stimulated by efforts to overcome the pharmacological problem of the high toxicity of cisplatin.[10]

In comparison with cisplatin complexes, their Pt^{IV} analogs consist of six-coordinate Pt^{IV} octahedral units. Because of this coordination geometry, ligand substitution is done mainly by a dissociative mechanism instead of the associative action that takes place in Pt^{II} complexes (e.g., cisplatin). Hence the replacement of the ligand is more demanding in the Pt^{IV} complexes.[11] As a matter of fact, this modification induces greater stability, which is desirable for achieving lower toxicity than cisplatin, and for potential oral bioavailability. Unfortunately, the steric arrangement of the Pt^{IV} is less favorable for interaction with double-stranded DNA. Despite this fact, Pt^{IV} complexes show strong antitumor properties.[12] This contradiction can be rationalized by anticipating in vivo reduction of the Pt^{IV} to Pt^{II}, which is more likely to interact with genetic material.[13] In other words, the lower toxicity and relative inertness of Pt^{IV} compounds can be used to overcome a crucial drawback of cisplatin applications by getting the drug to the desired place in the tissue before the Pt^{II} complex which can interact with DNA is generated, thus minimizing the unwanted side effects. On the basis of this idea, a range of Pt^{IV} complexes have been reported, characterized, and tested for their biological effects.[14−16]

Purine nucleobases and purine analogs are very promising as ligands of both Pt^{II} and Pt^{IV} complexes[17,18] and could also

Received: July 25, 2011
Published: January 19, 2012

   dx.doi.org/10.1021/ic201595e | Inorg. Chem. 2012, 51, 1371−1379

serve as appropriate models for better understanding interactions with DNA. A special class of purine derivatives, the aromatic cytokinins,[19] work as plant-growth promoting substances[20] by regulating cell division.[21] 6-Benzylaminopurine (BAP) is probably the most extensively investigated representative of this group (Figure 1). BAP derivatives and their

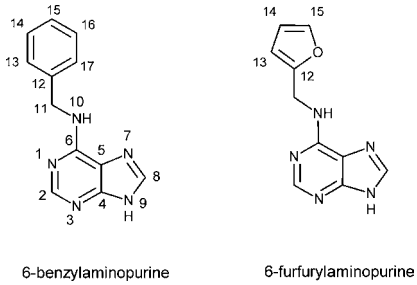

Figure 1. Structure and numbering scheme for 6-benzylaminopurine (BAP) and 6-furfurylaminopurine (kinetin, KIN).

transition-metal complexes have been tested for cytotoxicity[22,23] and are reported to be promising inhibitors of cyclin-dependent kinases (CDK). 6-Furfurylaminopurine (Kinetin, KIN, Figure 1), another member of this class of compounds, was isolated from autoclaved DNA as the first purine-based cytokinin in 1955.[24] It was considered to be only an artificial product until it was found to be present in plant tissue[25] and even in human urine.[26] Kinetin has been shown to have significant antiaging properties[27] and is currently widely used in the cosmetics industry.

While noting the biological relevance, one should keep in mind the crucial roles of the protonation, tautomerism, and proton-exchange processes which are characteristic of purine derivatives. Generally, proton transfer phenomena are the keystones for a myriad of important biomolecular processes in living tissue.[28] The protonation equilibria of the nucleobases are fundamental to their biological functions in several highly important biological systems, such as nucleic acids[29] (e.g., mode of base pairing), energy storage systems (e.g., enzymatically catalyzed ATP hydrolysis or synthesis), and reaction catalysts in biosystems. The biological implications of these tautomeric and protonation phenomena have been investigated thoroughly over the years.[30,31] Protonation of a nucleobase changes the distribution of the electron density in the purine ring, thus affecting the aromaticity and charge distribution of the molecule, which subsequently results in dramatic differences in reactivity between the deprotonated, neutral, and protonated forms. Further, the different forms are capable of creating different hydrogen-bonding patterns, resulting in variations in the stability of the supramolecular assembly, for example, the stability of systems containing A-T or G-C base pairs.[32]

Determination of the protonation patterns and coordination sites thus plays a crucial role in the chemistry of purine bases and their complexes.[17,33] Knowledge of their protonation equilibria allows us to interpret and predict their modes of binding to biological targets (nucleic acids, proteins)[34,35] and to better understand the biological processes in living organisms.

In this contribution, we investigate the Pt^{IV} coordination and protonation sites for BAP and KIN using state-of-the-art structural approaches that combine X-ray diffraction and NMR spectroscopy in solution and in the solid state with relativistic DFT calculations of structures and NMR parameters. Our data have unequivocally established the structures of compounds **1**; 9-[6-(benzylamino)purine] pentachloroplatinate (IV), [$Pt^{IV}Cl_5$BAPH]; and **2**; 9-[6-(furfurylamino)purine] pentachloroplatinate (IV), [$Pt^{IV}Cl_5$KINH]; shown in Figure 2. We

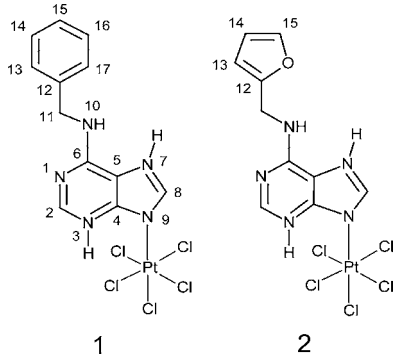

Figure 2. Structure and numbering scheme for compounds **1** and **2**.

report for the first time an X-ray characterized coordination bond between platinum(IV) and nitrogen atom N-9 of the purine base. In addition, the protonation patterns characterized here clearly contrast with those reported previously.[23,36]

2. EXPERIMENTAL SECTION

2.1. Chemicals and Preparation of Compounds 1 and 2. K_2PtCl_6 was purchased from Safina, 6-benzylaminopurine and kinetin (6-furfurylaminopurine) were supplied by Fluka, and *N*,*N*-dimethylformamide-d_7 (99.9% D) for NMR spectroscopy was purchased from Sigma-Aldrich and used without further purification. Infrared spectra were measured on a Bruker Vertex 80v spectrometer.

9-[6-(Benzylamino)purine] Pentachloroplatinate (IV). 6-Benzylaminopurine (0.11 g, 0.5 mmol) was dissolved in 2 M HCl (50 mL) and added to a solution of K_2PtCl_6 (0.24 g, 0.5 mmol) dissolved in 2 M HCl (30 mL). The solution was stirred under reflux at 50 °C for 4 h. The yellow precipitate of compound **1** was filtered, washed with water, and dried in air. Compound **1** was obtained in 60% yield. The crystal for single-crystal X-ray diffraction analysis was prepared by recrystallizing compound **1** from dimethylformamide (DMF). The DMF was evaporated at low pressure in a sealed vessel connected to a vacuum pump. The crystals were kept in the absence of light with the drying agent P_4O_{10} present in the vessel.

IR (ν, cm^{-1}): 3310 (N−H), 3055 (C_{ar}−H), 1645 (C═N), 538 (Pt−N), 364 (Pt−Cl).

^1H, ^{13}C, and ^{15}N NMR chemical shifts of the purine moiety are summarized in Table 1; chemical shifts of the benzyl part: ^1H NMR (δ, ppm): 4.98 (H11, d, $^4J_{H-H}$ = 6 Hz, 2H), 7.28 (H15, t, $^3J_{H15-H14}$ = 7.2 Hz, 1H), 7.35 (H14 and H16, dd, $^3J_{H14-H13}$ = 7.5 Hz, $^3J_{H14-H15}$ = 7.2 Hz, 2H), 7.47 (H13 and H17, d, $^3J_{H13-H14}$ = 7.5 Hz, 2H); ^{13}C (δ, ppm): 45.3 (C11), 128.3 (C15), 128.8 (C13 and C17), 129.6 (C14 and C16), 139.1 (C12); ^{195}Pt (δ, ppm): 120.

9-[6-(Furfurylamino)purine] Pentachloroplatinate (IV). Compound **2** was prepared analogously to compound **1**. Kinetin (0.10 g, 0.5 mmol) was dissolved in 2 M HCl (20 mL) and added to a solution of K_2PtCl_6 (0.24 g, 0.5 mmol) dissolved in 2 M HCl (30 mL). A yellow powder was obtained in 90% yield.

IR (ν, cm^{-1}): 3300 (N−H), 3045 (C_{ar}−H), 1640 (C═N), 542 (Pt−N), 368 (Pt−Cl). ^1H, ^{13}C, and ^{15}N NMR chemical shifts of the purine moiety are summarized in Table 1; chemical shifts of furfuryl part: ^1H NMR (δ, ppm): 5.00 (H11, d, $^4J_{H-H}$ = 5.3 Hz, 2H), 6.43 (H13, multiplicity unresolved, 1H), 6.49 (H14, unresolved, 1H), 7.65 (H15, unresolved, 1H); ^{13}C (δ, ppm): 38.5 (C11), 108.7 (C13), 111.2 (C14), 143.4 (C15), 151.6 (C12); ^{195}Pt (δ, ppm): 108.

2.2. NMR Spectroscopy in Solution. The ^1H, ^{13}C, and ^{15}N NMR spectra were recorded on a Bruker Avance 500 spectrometer operating at frequencies of 500.13 MHz (^1H), 125.77 MHz (^{13}C), and 50.68 MHz (^{15}N). The compounds were dissolved in

dx.doi.org/10.1021/ic201595e | Inorg. Chem. 2012, 51, 1371−1379

Table 1. ^{1}H, ^{13}C, and ^{15}N NMR Chemical Shifts (ppm) for Compounds 1 and 2 at 303 K

	1			2		
atom	solid state	DMF	DMF with HCl	solid state	DMF	DMF with HCl
C2	148.8	145.7	147.3	149.4	146.0	147.2
C4	140.7	144.4	142.3	141.0	143.8	142.7
C5	111.0	120.1	113.1	111.2	117.9	114.3
C6	152.2	156.1	153.5	152.5	155.0	153.8
C8	144.2	149.4	145.3	145.8	148.5	146.2
N1	227.7	225.2	227.7	229.0	226.6	228.1
N3	152.7	153.5	152.9	153.1	153.8	153.4
N7	165.4	227.2	180.8	164.5	211.2	185.3
N9	141.5	136.9	144.0	141.0	139.8	144.0
N10	121.5	106.9	*a*	119.0	105.5	114.7
H2	*b*	8.73	8.91	*b*	8.84	8.92
H8	*b*	8.38	9.18	*b*	8.62	9.07

[a]Not observed. [b]Not measured.

N,*N*-dimethylformamide-d_7 at concentrations of 5 mg/mL for **1** and 15 mg/mL for **2**. The ^{1}H and ^{13}C NMR chemical shifts (δ in ppm) were referenced to the signal of the solvent [8.01 ppm for residual DMF-d_6 (^{1}H); 162.7 ppm for DMF-d_7 (^{13}C)]. The ^{15}N NMR chemical shifts were referenced to external 1 M urea in DMSO-d_6 (77.0 ppm)[37] and are reported relative to liquid ammonia.[38,39] The ^{195}Pt NMR spectra were recorded on a Bruker Avance 300 spectrometer operating at frequencies of 300.13 MHz for ^{1}H and 64.52 MHz for ^{195}Pt. $[PtCl_6]^{2-}$ in D_2O was used as an external reference (0 ppm).[40] The NMR spectra were obtained at temperatures between 233 and 303 K, as specified in the text. A set of 2D NMR experiments was used to assign the individual ^{1}H, ^{13}C, and ^{15}N resonances: ^{1}H-^{13}C gs-HSQC,[41,42] ^{1}H-^{13}C gs-HMBC,[43,44] ^{1}H-^{13}C GSQMBC, and ^{1}H-^{15}N GSQMBC.[45]

2.3. Solid-State NMR Spectroscopy. The solid-state NMR experiments were performed at ambient temperature on a Bruker AVANCE 500 spectrometer operating at frequencies of 500.13 MHz for ^{1}H and 125.77 MHz for ^{13}C. A Bruker 4 mm CP/MAS probe was used for all of the measurements. The ^{13}C CP/MAS spectra were recorded with a 3 ms contact time and an optimized recycle delay of 20 s for **1** and 30 s for **2**. The ramped-amplitude (RAMP) shape pulse was used during the cross-polarization and two-pulse phase-modulated (TPPM) decoupling during the acquisition. A CPPI experiment was performed to assist in assigning the ^{13}C NMR chemical shifts. Crystalline α-glycine was used as a secondary reference (δ_{st} = 176.03 ppm for $^{13}C_{C=O}$ and δ_{st} = 34.1 ppm for ^{15}N).[46,47]

2.4. Single-Crystal X-ray Diffraction. The diffraction data were collected with a Kuma-KM4 four-circle κ-axis diffractometer equipped with a CCD detector and an Oxford Cryostream Cooler (Oxford Cryosystems, U.K.). Molybdenum Kα radiation (λ = 0.71073 Å, monochromator Enhance, Oxford Diffraction, U.K.) was used for all measurements. We performed the ω-scan technique with different values of κ and ϕ to cover the entire independent part of the reflections. Data collection, cell parameters, data reduction, and correction procedures were carried out using the programs CrysAlis CCD and CrysAlis RED (Oxford Diffraction, U.K.). The phase problem was solved by direct methods using the program SIR2002.[48] The program SHELXL-97[49] was used to refine the structure by using a full-matrix least-squares procedure on F^2. All non-hydrogen atoms were refined as independent atoms using anisotropic thermal parameters. All of the H atoms were located in a difference map and refined using a riding model. The crystal had a block shape and was orange. The dimensions of the crystal were 0.25 × 0.20 × 0.15 mm.

Crystal data for **1**: CCDC no. 827979, $P2_1/n$, a(Å) = 15.1279(4), b(Å)= 8.3336(3), c(Å) = 20.7956(6), β(deg) = 100.496(3), Z = 4, V(Å^3) = 2577.83(14), T(K) = 120(2), $\rho_{min/max}$ (e/Å^{-3}) = −0.661/1.648, R_{gt} = 0.0228, R_{all} = 0.0287, reflections collected: 29609, independent reflections: 4528, observed reflections ($I > 2\sigma(I)$): 3875, number of parameters: 302, absorption correction type: multiscan, μ = 5.992 mm^{-1}, T_{min} = 0.469, T_{max} = 1.000.

2.5. DFT Calculations. Geometry optimizations were performed at the density-functional theory (DFT) level using a B3LYP[50,51] functional with a 6-31G* basis set for light atoms[52] and relativistic effective core potentials (ECP60MDF and ECP60MDF_wcVTZ) for platinum.[53] A harmonic frequency analysis was performed to verify the calculated energy minima. The geometry optimizations were performed using the Gaussian 03 package[54] and the optimized structures were used to further calculate the nuclear magnetic shielding using the Gauge Including Atomic Orbitals (GIAO) method.[55] A B3LYP functional and an ECP60MDF with a cc-pVTZ-PP basis set were used for platinum and an IGLO-III-UT3 basis set for light atoms.[56,57] The polarizable-continuum model (PCM)[58,59] with standard G03 parameters for DMF was used to calculate both the geometry and the nuclear magnetic shielding.

The all-electron approach with a zeroth-order regular approximation and incorporating spin−orbit coupling (ZORA-SO)[60,61] as implemented in the ADF-2009[62] program was used. The PBE0 hybrid GGA functional with a somewhat increased exact-exchange admixture (30%)[57] and a TZP basis set from the standard ADF library were employed. A COSMO model[63] (with standard ADF parameters for DMF) was used to simulate the effects of the solvent on the nuclear magnetic shielding.

3. RESULTS AND DISCUSSION

Compounds **1** and **2** were each prepared in one step by mixing the corresponding base with K_2PtCl_6 under acidic conditions. The general structure of these complexes can be described as the zwitterion $[Pt^{IV}Cl_5LH]$ where LH^+ represents the protonated ligand (BAP or KIN) compensating the negatively charged $PtCl_5$ unit. Generally, characterizing the protonation patterns of the purine bases in solution is complicated by equilibria among several forms. To eliminate this behavior, we started by characterizing the structure in the solid state using solid-state NMR spectroscopy and X-ray diffraction.

3.1. Solid-State Structure. The ^{13}C NMR chemical shifts (see Table 1) were obtained from a CP/MAS experiment and assigned with the help of CPPI (see Experimental Section). The chemical shifts obtained for the bridgehead carbons C4 and C5 indicate that the nitrogen atoms N3, N7, and N9 are either trapped in the Pt−N coordination bond or protonated (see Table 1). In contrast, the chemical shift of C6 points to the presence of a bare (nonsubstituted) nitrogen atom N1.[33]

To obtain additional information about the suggested pattern, the ^{15}N CP/MAS spectrum at the natural abundance of the ^{15}N isotope was measured. Two of the five observed ^{15}N resonances can be assigned easily on the basis of their chemical shifts. The only resonance with a chemical shift exceeding 200 ppm—indicating that this nitrogen is bare[38,39]—was assigned to N1.

This assignment is consistent with the NMR measurements in solution and the results of the X-ray diffraction analysis (vide infra). The second signal of this pair is that of the NH group in the benzylamino-(furfurylamino-) side chain, with a chemical shift located at $\delta \sim 120$ ppm. The other three signals fall into the range of 140−165 ppm, which points to the involvement of these nitrogen atoms in protonation or complexation.[38,39] The ^{15}N NMR resonance at ∼141 ppm differs from the remaining two resonances by a line width (signal broadening). This phenomenon is attributable to spin−spin coupling with the ^{195}Pt (indirect nuclear spin−spin coupling, not resolved).

dx.doi.org/10.1021/ic201595e | Inorg. Chem. 2012, 51, 1371−1379

On the basis of findings obtained from X-ray diffraction and NMR spectroscopy in solution (vide infra), this signal was assigned to the N9 atom. The two ^{15}N resonances at ~153 ppm and ~165 ppm cannot be assigned experimentally in a straightforward way. Therefore, solution-state NMR data and DFT calculations of the chemical shifts were used to assign these resonances (see following sections 3.2 and 3.4).

In addition, the structure of compound **1** in the solid state was characterized by single-crystal X-ray diffraction. A suitable single crystal was prepared by crystallizing compound **1** from dimethylformamide to yield the solvate **1**·$(DMF)_2$. In accordance with the solid-state NMR measurements, the molecular structure was confirmed to consist of $BAPH^+$ and octahedral $[PtCl_5]^-$ units coupled together by a bond between N9 and Pt. To the best of our knowledge, this is the first report unequivocally charaterizing any purine base modified with Pt^{IV} at position N9. The molecular structure of compound **1** determined by X-ray diffraction is shown in Figure 3.

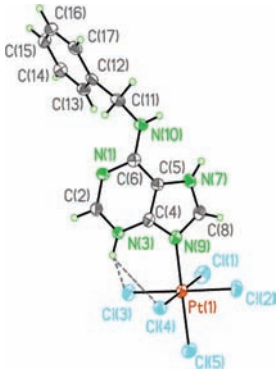

Figure 3. ORTEP drawing of the molecular structure of $Pt^{IV}Cl_5BAPH$ (**1**) with atom numbering; the stabilizing intramolecular N−H···Cl interactions are highlighted.

Intramolecular hydrogen bonds between N3−H and the Cl3 and Cl4 atoms are highlighted in the figure, and their role in stabilizing the hydrogen atom at N3 in solution is thoroughly discussed in the following chapter. A portion of the crystal structure with selected intermolecular hydrogen bonds and $\pi-\pi$ stacking interactions is shown in Figure 4.

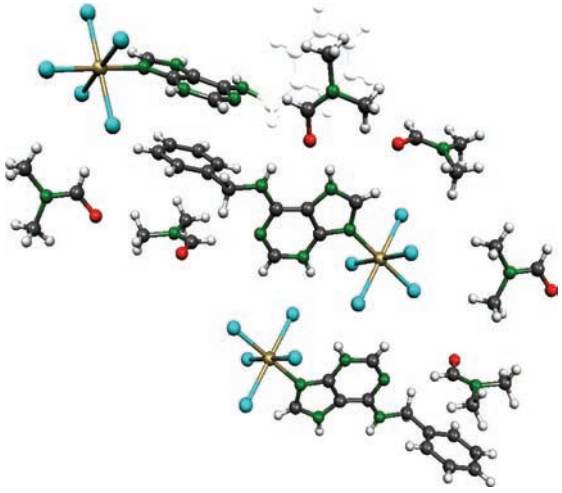

Figure 4. Crystal packing for **1**·$(DMF)_2$.

The crystal structure is stabilized by the hydrogen bonding of the oxygen atom of DMF with two N−H groups of the complex (N7−H and N10−H). In addition, $\pi-\pi$ interaction between the purine ring and the benzyl moiety of the neighboring molecule stabilizes the crystal structure of **1**·$(DMF)_2$.

3.2. Structure in Solution. Although the protonation pattern in the solid state has been determined by complementary analysis using X-ray diffraction and solid-state NMR spectroscopy, the protonation model in solution can be substantially different from that observed in the solid state. In principle, the presence of three nitrogen protonation sites in the purine core (N1, N3, and N7; N9 is occupied by the Pt atom) together with the two imino protons (for the neutral complex) can generate three tautomeric forms A, B, and C (see Figure 5).

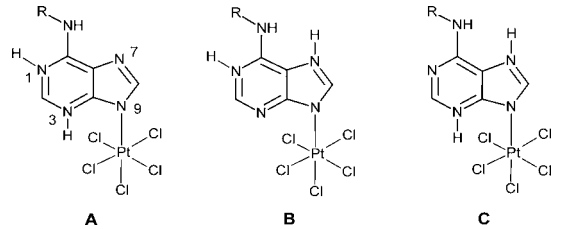

Figure 5. Three theoretical tautomers for the N9-platinated neutral complexes **1** and **2**.

To characterize the structures of **1** and **2** in DMF solution unequivocally, we performed extensive NMR analysis employing ^1H, ^{13}C, ^{15}N, and ^{195}Pt nuclei. The ^1H and ^{13}C NMR resonances were assigned on the basis of gradient-selected HSQC, gs-HMBC, and GSQMBC experiments (see Table 1). The results correlate nicely with the assignments for other purine derivatives reported previously.[19,33,39,64,65]

The signal of H8 is somewhat broadened because of the chemical exchange processes occurring in the DMF solution at ambient temperature. However, the H8 resonance is notably sharpened at a temperature of 233 K, allowing the unequivocal assignment of H8 based on its specific long-range ^1H-^{13}C interaction with the characteristically shielded signal of C5 (for experimentally obtained indirect nuclear spin−spin coupling constants, see Table 2).

Table 2. Selected Indirect Nuclear Spin−Spin Coupling Constants J_{IS} (Hz) for Compounds 1 and 2

	1		2	
I−S	DMF	DMF with HCl	DMF	DMF with HCl
H2−C4	8.0	8.6	8.0	8.3
H2−C6	11.9	12.6	11.7	12.0
H8−C4	8.1	9.4	8.8	9.3
H8−C5	11.1	8.4	10.2	8.5
H2−N1	15.0	14.5	14.6	14.5
H2−N3	7.4	7.4	7.0	7.4
H8−N7	14.8	7.9	10.5	8.4
H8−N9	7.8	7.4	8.4	8.0
H8−Pt	8.9	12.7	9.5	12.6
C8−Pt	18.0	*a*	19.3	*a*
N9−Pt	*a*	330.0	340.0	328.0

[a]Not observed.

dx.doi.org/10.1021/ic201595e | *Inorg. Chem.* 2012, 51, 1371−1379

In addition, we obtained satellite signals for H8 arising from its indirect spin−spin interaction with Pt-195 ($^3J_{Pt-H8}$ = 8.9 Hz). Portions of the ^{1}H NMR spectra for compound **2** in DMF-d_7 and in DMF-d_7 to which a of drop of HCl has been added highlight the shift of the H8 resonance and are shown in Figure 6. The fact that no interaction between H2 and Pt was

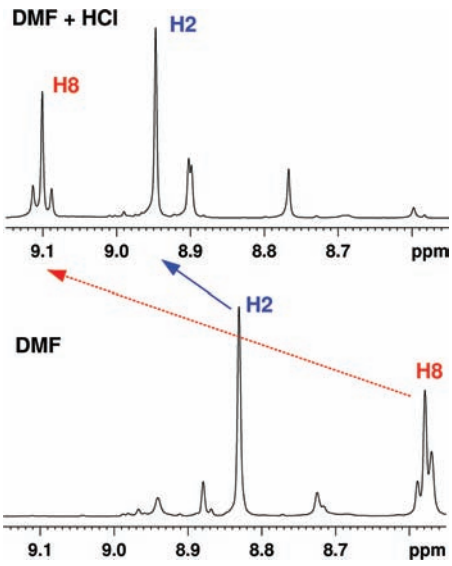

Figure 6. Portion of the ^{1}H NMR spectrum of compound **2** recorded in DMF-d_7 (bottom) and DMF-d_7+HCl (top) at 283 K: notice the ^{195}Pt satellites of the H8 resonance.

observed unambiguously confirms the coordination of the Pt atom to the imidazole part of the purine system. Further, the observation of ^{195}Pt satellites for carbons C4 (only partially resolved) and C8 ($^2J_{Pt-C}$ = 18 Hz) indicates that Pt is coordinated at the N9 atom, in accordance with the solid-state structure characterized by using X-ray diffraction.

To further support our findings and to obtain additional information about protonation patterns in solution, ^{15}N NMR spectra at the natural abundance of the ^{15}N isotope were measured indirectly using ^{1}H-^{15}N long-range chemical shift correlations. A portion of the ^{1}H-^{15}N GSQMBC spectrum for compound **2** measured at 283 K is shown in Figure 7. We

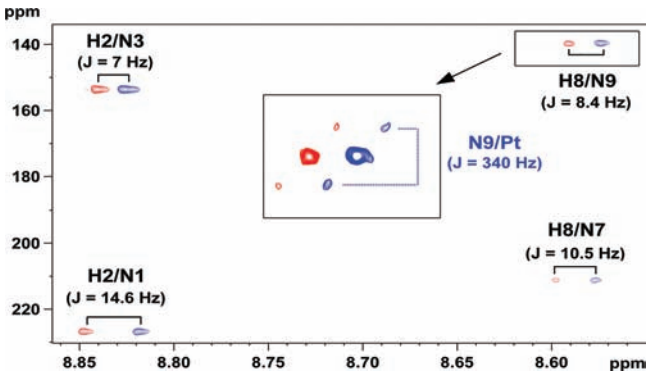

Figure 7. Portion of the ^{1}H-^{15}N GSQMBC spectrum of **2** in DMF-d_7 at 283 K with additional details of the N9−H8 correlation highlighting the ^{15}N−^{195}Pt interaction.

observed the signals of all four nitrogen atoms of the purine skeleton in the ^{1}H-^{15}N GSQMBC spectrum recorded at 283 K, but the signal of N10−H was missing from the spectrum. However, this resonance was detected, when the same experiment was performed at 263 K. Generally, the observed ^{15}N NMR chemical shifts (see Table 1) were very similar to those measured in the solid state with one exception, where a dramatic difference was obtained (vide infra).

The most shielded ^{15}N resonances occurred at 136.9 ppm for **1** and 139.8 ppm for **2**, correlating with the H8 signals and clearly showing resolved ^{195}Pt satellites (see Figure 7). These have been straightforwardly assigned to the respective N9 atoms. A detailed examination of the ^{1}H-^{15}N chemical shift correlation spectra showed a weak four-bond interaction of the N9 resonance with H2 ($^4J_{N9-H2}$ = 1.5 Hz).[33,66] This unequivocally confirmed the assignment of the N9 resonances because the five-bond H2−N7 interactions are vanishingly small and typically are not observed for purine-based compounds. As a consequence, the second ^{15}N signal of the imidazole part correlating with H8 must belong to the N7 atom. However, we observed a dramatic difference between its NMR chemical shift in solution (∼ 220 ppm) and in the solid state (∼ 165 ppm). This behavior is discussed thoroughly in the subsequent section 3.3.

From the two ^{15}N signals correlating with H2, we clearly identified the signals at 225.2 ppm for **1** and 226.6 ppm for **2** as belonging to N1. This assignment is based on the correlation detected between the hydrogen atom N10−H and the atom N1 with $^3J_{N-H}$ = 6.1 Hz for **1** and $^3J_{N-H}$ = 5.7 Hz for **2** (at 263K). The chemical shifts of ∼226 ppm for the N1 atom unambiguously indicate a bare nitrogen and preclude the presence of tautomers A and B in the DMF solution.

The second signal correlating with H2 is particularly shielded (δ ∼153 ppm) and was assigned to the protonated nitrogen N3. The ^{15}N NMR chemical shift of N3 is almost identical in solution and in the solid state ($\Delta\delta$ ∼ 0.7 ppm) and thus seems to be environment invariant, which suggest that any effects of the crystal packing and solvation on the nuclear shielding are marginal. This invariance could be explained by the presence of some intramolecular stabilizing interaction involving the N3−H hydrogen atom. Analysis of the X-ray structure reveals the proximity of N3−H and two chlorine atoms of the $PtCl_5$ unit. Because X-ray crystallography is rather inaccurate in determining the positions of hydrogen atoms, we employed DFT calculations to investigate the possibility of such assumed intramolecular stabilizing interactions. Because of the presence of a heavy atom in the system we investigated, the relativistic effects on the molecular topology calculated using DFT were treated by using relativistic effective core potentials (ECP, for details see Experimental Section). The interatomic distances N3-**H···Cl3** and N3-**H···Cl4** of around 2.7 Å were extracted from the DFT-optimized structures of **1** and **2**. Our value (∼2.7 Å) is notably smaller than the sum of the van der Waals radii (2.95 Å) reported for H (1.2 Å) and Cl (1.75 Å).[67] This fact together with the absence of any chemical exchange process that would affect the ^{15}N NMR resonance of the N3−H moiety in solution points to the presence of the stabilizing intramolecular interactions N3-**H···Cl3** and N3-**H···Cl4**. Very recently, analogous N−H···Cl interactions have been reported for Ir^{III} and Ru^{III} complexes of purine bases.[68,69] However, we have not been able to characterize these interactions more precisely by determining the electron density at the hydrogen-bond critical point (ρ_{HBCP}) because of the presence of the Pt atom in the system.

In clear contrast to the observations for the N3 signal, the significantly deshielded ^{15}N resonance of N-7 (δ > 200 ppm in

dx.doi.org/10.1021/ic201595e | Inorg. Chem. 2012, 51, 1371−1379

DMF solution) indicates a notable weakening of the bond N7−H, resulting in at least partial deprotonation of this nitrogen atom in DMF solution. This phenomenon induced us to consider and investigate the possibility that dynamic tautomeric and protonation equilibria might exist in DMF solution.

3.3. Protonation Equilibria in Solution. As described in the previous section, for the four nitrogen sites of the purine core, we assume the presence of two protonated sites N3 and N7, one bare nitrogen atom N1, and the platinated N9. Whereas the hydrogen atom at N3 has been confirmed to be relatively stable because of the presence of a stabilizing intramolecular interaction with the chlorine atoms, the chemical shift of N7 indicates substantial lability of the N7−H bond under the experimental conditions (DMF solution).

To influence the protonation/deprotonation equilibrium involving the N7 atom, we added a small amount of HCl to the DMF solutions of **1** and **2** (with final concentration <0.1 M HCl). A dramatic change in the ^{15}N NMR chemical shift of N7, together with changes for H8 and C5, was then observed (Table 1). In contrast, the chemical shift of N3 was practically unaffected by the amount of acid in the solution. Both facts support our previous assumptions. To estimate the degree of protonation at N7 for the two samples analyzed (in DMF-d_7 and in DMF-d_7 with added HCl) we had to employ either NMR titration experiments or the NMR chemical shifts calculated for the selected atoms in two "limit" states (fully protonated and fully deprotonated at N7). First, we tried to reach this goal experimentally by adding acid or base to solutions of **1** and **2**. However, higher concentrations of acid (>0.1 M HCl) led to the precipitation of the complexes, whereas addition of the base (Na_2CO_3) resulted in the decomposition of both complexes. Therefore, we turned to an indirect approach and employed DFT calculations to determine the NMR parameters of the two "limit" states for each compound.

3.4. Relativistic DFT Calculations of Nuclear Magnetic Shielding. The geometries of all of the structures were optimized at the DFT level using the Gaussian03 package with a B3LYP functional and a 6-31G* basis set for light atoms (see Experimental Section). For platinum, as a heavy element, we employed the effective core potential approach, which speeds up the calculations as compared to the full-electron basis sets, produces the data with similar accuracy, and, in addition, incorporates scalar-relativistic corrections. The geometries were first optimized in vacuo and subsequently reoptimized using the polarizable-continuum model (PCM) with DMF as the solvent.

To support our previously formulated structural conclusion that form C (N3H/N7H, Figure 5) predominates over form A (N1H/N3H), we calculated the heats of formation of forms A and C (the B form is excluded because of unequivocal evidence of protonation at the N3 atom). The differences in energy (−19.6 kcal/mol for **1** and −15.5 kcal/mol for **2**) clearly favor tautomeric form C (N3H/N7H), which corresponds to the structural conclusions drawn from the experimental NMR data.

Considering the assumed partial deprotonation at N7 in solution, we carried out calculations for a negatively charged molecule created from tautomeric form C by subtracting the proton from N7−H. The DFT-optimized geometries for both of these "limit" states of **2** are shown in Figure 8.

In a subsequent step, the optimized geometries of the N3H and N3H/N7H forms were used for GIAO nuclear magnetic shielding calculations employing the PCM solvent model. The presence of a heavy element (Pt), however, required that relativistic corrections be incorporated in the nuclear magnetic shielding calculations. Including scalar-relativistic (SR) effects by applying the relativistic effective core potentials (ECPs) improved the agreement with experiment as compared to the nonrelativistic shielding only marginally (data not shown).

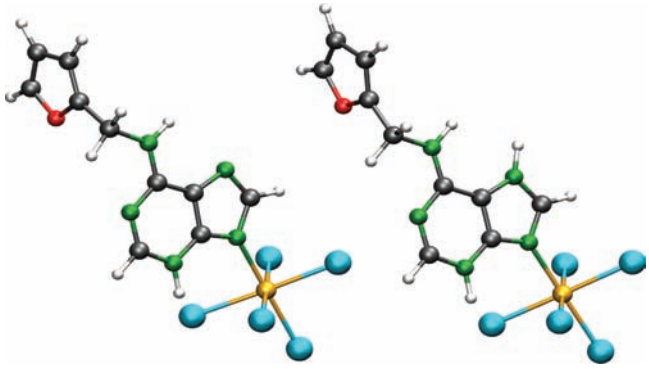

Figure 8. Molecular structures of the N3H (left) and N3H/N7H (right) forms of **2** optimized at the B3LYP/ECP60MDF/6-31G* level (for details, see Experimental Section).

On the contrary, spin−orbit (SO) corrections to the NMR chemical shifts[70−73] showed themselves to be quite significant, particularly for the N9 atom directly bonded to the metal center. We used the zeroth-order regular approximation (ZORA), with spin−orbit coupling included (ZORA-SO), as implemented in the ADF-2009 software (see Experimental Section). Employing this approach diminished the difference between the experimental and the calculated chemical shift for the N9 atom from ∼35 ppm (ZORA-SR) down to ∼10 ppm (ZORA-SO) in the case of **2**, as evident from the data summarized in Table 3.

3.5. Population of N3H/N7H Form and Population-weighted NMR Chemical Shifts. Because the calculated chemical shift values for atoms distant from the Pt center (e.g., C2, C4, and N3 with marginal SO corrections) are in acceptable agreement with experiment for both forms (marginal effects of protonation), we consider our approach as validated. One should keep in mind that the theoretical NMR data are calculated for the negatively charged N3H or the completely protonated N3H/N7H form, whereas the experimental values correspond to the population-weighted contributions of the N3H and N3H/N7H forms. In the next step, the theoretical NMR chemical shifts for the N7 atom in the two "limit" states N3H (0% in Figure 9) and N3H/N7H (100% in Figure 9) have been used to estimate the population of the N3H/N7H form in the DMF and DMF+HCl solutions. The dependence of the weighted chemical shift of the N7 atom on the population of the N3H/N7H form (degree of protonation) for **2** is shown graphically in Figure 9. We can estimate from Figure 9 that the N7 atom in **2** is approximately 38% protonated in DMF solution, while the addition of a drop of HCl increases the population of the N3H/N7H form to 67%. Similar results were obtained for complex **1** in DMF with HCl (71%), although a significantly different ratio was detected for the DMF solution (∼ 15%). This seemingly different behavior for **1** and **2** in DMF can, however, be explained in a straightforward way by the much lower concentration of **1** in the DMF solution (because of lower solubility), resulting in a greater degree of deprotonation under these conditions.

The population of the N3H/N7H form estimated for the DMF solution (38%) from Figure 9 was used to calculate the

dx.doi.org/10.1021/ic201595e | Inorg. Chem. 2012, 51, 1371−1379

Table 3. DFT Calculated and Experimental NMR Chemical Shifts (ppm) for Compound 2 in DMF Solution

	N3H form			N3H/N7H form				
	ZORA-SR[a]	SO[b]	ZORA-SO[c]	ZORA-SR[a]	SO[b]	ZORA-SO[c]	weighted average	experimental
C2	145.5	−1.1	144.4	146.9	−0.9	146.0	145.0	146.0
C4	144.3	−1.8	142.5	143.2	−0.9	142.3	142.4	143.8
C5	121.7	−0.5	121.2	112.6	−0.5	112.1	117.7	117.9
C6	153.4	−0.9	152.5	151.7	−1.0	150.7	151.8	155.0
C8	153.9	−2.0	151.9	146.1	−2.1	144.0	148.8	148.5
rmsd[d]	**3.0**		**2.5**	**3.0**		**3.9**	**1.6**	-
N1	229.2	−1.1	228.1	235.9	−1.2	234.7	230.7	226.6
N3	153.6	−1.4	152.2	153.1	−1.6	151.5	151.9	153.8
N7	247.7	−1.4	246.3	156.9	−1.8	155.1	211.2	211.2
N9	173.3	−26.4	146.9	176.3	−22.3	154.0	149.6	139.8
N10	94.4	−1.3	93.1	119.9	−1.4	118.5	102.9	105.5
rmsd[d]	**22.7**		**17.0**	**30.3**		**26.8**	**5.0**	

[a]One-component ZORA (scalar-relativistic, SR). [b]Spin−orbit correction. [c]Two-component ZORA (SR+SO). [d]Root-mean-square deviation.

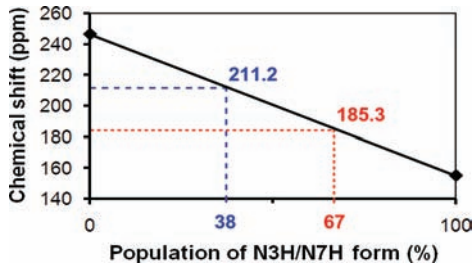

Figure 9. DFT calculated ^{15}N NMR chemical shift for the N7 atom in the N3H (at 0%) and the N3H/N7H (at 100%) forms of compound **2**. The experimentally determined chemical shifts for the DMF-d_7 and DMF-d_7+HCl solutions are highlighted with blue and red lines, respectively.

remaining population-weighted ^{13}C and ^{15}N NMR chemical shifts (see Table 3). The population-weighted averaging of chemical shifts produced results very similar to those observed in solution, as shown by the root-mean-square deviation (1.6 ppm for ^{13}C and 5.0 ppm for ^{15}N). This in turn supports the reliability of the DFT approach employed here and the structural conclusions formulated.

4. CONCLUSIONS

New Pt^{IV} complexes with aromatic cytokinins have been prepared, and their coordination and protonation sites have been determined unequivocally by NMR spectroscopy, X-ray diffraction, and relativistic DFT calculations.

In the solid state, the structure of **1** was characterized by single-crystal X-ray diffraction, which established that the platinum was unprecedentedly coordinated to N9. Analysis of the ^{13}C and ^{15}N CP/MAS NMR data unexpectedly established that the protonation pattern is N3H/N7H—in clear contrast to previous reports.[23,33] The identical coordination/protonation pattern (N9Pt/N3H/N7H) was determined in solution by 2D NMR spectroscopy and DFT calculations. The inclusion of the scalar-relativistic and spin−orbit effects was indispensable for calculating the nuclear shielding of the individual atoms and obtaining the theoretical chemical shifts for the individual species (neutral N3H/N7H and anionic N3H). Clearly, the N3H proton is very stable in solution and is scarcely involved in the protonation/deprotonation equilibrium. The stability of the N3H proton can be structurally rationalized by the presence of a stabilizing interaction between N3H and the chlorine atoms of the $[PtCl_5]^-$ moiety. Surprisingly, but unambiguously, the N7H site proved to be the most sensitive to deprotonation. More specifically, by employing the ^{15}N NMR chemical shifts for the N7 atom in the neutral N3H/N7H tautomer (solid-state NMR, DFT calculations) and the anionic N3H form (DFT calculations), the degree of protonation at N7 was estimated to be approximately 38% for **2** in DMF solution, which increased to about 67% when the acidity of the medium was slightly increased. Our approach combining the experimental NMR spectroscopy and relativistic DFT calculations can be applied to a wide range of problems aiming at characterizing the tautomeric and protonation equilibria in purine ligands modified by metal binding.

■ ASSOCIATED CONTENT

Ⓢ Supporting Information

Crystallographic data in CIF format and further details on chemical shifts and geometries of structures. This material is available free of charge via the Internet at http://pubs.acs.org.

■ AUTHOR INFORMATION

Corresponding Author

*Phone: +420549495748. Fax: +420549492556. E-mail: rmarek@chemi.muni.cz.

Dedication

†Dedicated to Professor Jaroslav Jonas on the occasion of his 75th birthday.

■ ACKNOWLEDGMENTS

This research was financially supported by grants from the Czech Science Foundation (P206/11/0550 to R.M. and P206/12/0539 to J.V.) and the project "CEITEC−Central European Institute of Technology" (CZ.1.05/1.1.00/02.0068) from European Regional Development Fund. The computational resources were partially provided by the MetaCentrum, Czech Republic (under research Grant MSM6383917201).

■ REFERENCES

(1) Rosenberg, B.; Van Camp, L.; Krigas, T. *Nature* **1965**, *205*, 698−699.

(2) Kelland, L. R.; Farrell, N. P. *Platinum-Based Drugs in Cancer Therapy*; Humana Press: Totowa, NJ, 2000.

(3) Harrap, K. R. *Cancer Treat. Rev.* **1985**, *12*, 21−33.
(4) Pasetto, L. M.; D'Andrea, R. M.; Brandes, A. A.; Rossi, E.; Monfardini, S. *Crit. Rev. Oncol. Hematom.* **2006**, *60*, 59−75.
(5) Terzis, A. *Inorg. Chem.* **1976**, *15* (4), 793−796.
(6) Gielen, M.; Tiekink, E. R. T. *Metallotherapeutic Drugs and Metal-Based Diagnostic Agents*; Wiley: London, U.K., 2005, 399−419.
(7) Garoufis, A.; Hadjikakou, S. K.; Hadjiliadis, N. *Coord. Chem. Rev.* **2008**, *253*, 1384−1397.
(8) Hall, M. D.; Hambley, T. W. *Coord. Chem. Rev.* **2002**, *232*, 49−67.
(9) Rosenberg, B.; Vancamp, L.; Trosko, J. E.; Mansour, V. H. *Nature* **1969**, *222*, 385−386.
(10) Lippert, B., Ed.; *Cisplatin: Chemistry and Biochemistry of a Leading Anticancer Drug*; Wiley-VCH: Weinheim, Germany, 1999.
(11) Kraatz, H.-B.; Metzel-Nolte, N. *Concepts and Models in Bioinorganic Chemistry*; Wiley-VCH Verlag: Weinheim, Germany, 2006.
(12) Keppler, B. K., Ed.; *Metal Complexes in Cancer Chemotherapy*; Wiley-VCH Verlag: Weinheim, Germany, 1993.
(13) Weaver, E. L.; Bose, R. N. *J. Inorg. Biochem.* **2003**, *95*, 231−239.
(14) Sabo, T. J.; Dinovič, V. M.; Kaluderovič, G. N.; Stanojkovič, T. P.; Bogdanovič, G. A.; Juranič, Z. D. *Inorg. Chim. Acta* **2005**, *358*, 2239−2245.
(15) Kim, H. J.; Kim, K. M.; Song, R.; Sohn, Y. S. *Inorg. Chim. Acta* **2005**, *358*, 415−418.
(16) Hall, M. D.; Amjadi, S.; Zhang, M.; Beale, P. J.; Hambley, T. W. *J. Inorg. Biochem.* **2004**, *98*, 1614−1624.
(17) Maloň, M.; Trávníček, Z.; Marek, R.; Strnad, M. *J. Inorg. Biochem.* **2005**, *99*, 2127−2138.
(18) (a) Gaballa, A. S. *J. Mol. Struct.* **2006**, *782*, 204−208. (b) Gaballa, A.; Schmidt, H.; Wagner, C.; Steinborn, D. *Inorg. Chim. Acta* **2008**, *361*, 2070−2080.
(19) Vícha, J.; Maloň, M.; Veselá, P.; Humpa, O.; Strnad, M.; Marek, R. *Magn. Reson. Chem.* **2010**, *48*, 318−322.
(20) Holub, J.; Hanuš, J.; Hanke, D. E.; Strnad, M. *J. Plant Growth Regul.* **1998**, *26*, 109−115.
(21) Skoog, F.; Armstrong, D. J. *Annu. Rev. Plant Physiol.* **1970**, *21*, 359−384.
(22) Doležal, K.; Popa, I.; Kryštof, V.; Spíchal, L.; Fojtíková, M.; Holub, J.; Lenobel, R.; Schmulling, T.; Strnad, M. *Bioorg. Med. Chem.* **2006**, *14*, 875−884.
(23) Trávníček, Z.; Popa, I.; Čajan, M.; Herchel, R.; Marek, J. *Polyhedron* **2007**, *26*, 5271−5282.
(24) Miller, C. O.; Skoog, F.; Von Saltza, M. H.; Strong, F. M. *J. Am. Chem. Soc.* **1955**, *77*, 1392−1392.
(25) Raman, N.; Elumalai, S. *Indian J. Exp. Biol.* **1996**, *34*, 577−580.
(26) Barciszewski, J.; Mielcarek, M.; Stobiecki, M.; Siboska, G.; Clark, B. F. C. *Biochem. Biophys. Res. Commun.* **2000**, *279*, 69−73.
(27) Rattan, S. I. S.; Clark, B. F. C. *Biochem. Biophys. Res. Commun.* **1994**, *201*, 665−672.
(28) Hynes, J. T.; Klinman, J.; Limbach, H. H.; Schowen, R. L. *Hydrogen Transfer Reactions*; Wiley-VCH: Weinheim, Germany, 2007.
(29) Lippert, B.; Gupta, D. *Dalton Trans.* **2009**, 4619−4634.
(30) Legault, P.; Pardi, A. *J. Am. Chem. Soc.* **1997**, *119*, 6621−6628.
(31) McConnell, T. L.; Wheaton, C. A.; Hunter, K. C.; Wetmore, S. D. *J. Phys. Chem. A* **2005**, *109*, 6351−6362.
(32) Sahu, P. K.; Kuo, C. W.; Lee, S. L. *J. Phys. Chem. B* **2007**, *111*, 2991−2998.
(33) Marek, R.; Sklenář, V. *Annu. Rep. NMR Spectrosc.* **2005**, *54*, 201−242.
(34) Muller-Dethlefs, K.; Hobza, P. *Chem. Rev.* **2000**, *100*, 143−168.
(35) Sharif, S.; Fogle, E.; Toney, M. D.; Denisov, G. S.; Shenderovich, I. G.; Buntkowsky, G.; Tolstoy, P. M.; Huot, M. C.; Limbach, H. H. *J. Am. Chem. Soc.* **2007**, *129*, 9558−9559.
(36) Major, D. T.; Laxer, A.; Fischer, B. *J. Org. Chem.* **2002**, *67*, 790−802.
(37) Wishart, D. S.; Bigam, C. G.; Yao, J.; Abildgaard, F.; Dyson, H. J.; Oldfield, E.; Markley, J. L.; Sykes, B. D. *J. Biomol. NMR* **1995**, *6*, 135−140.
(38) Marek, R.; Lyčka, A. *Curr. Org. Chem.* **2002**, *6*, 35−66.
(39) Marek, R.; Lyčka, A.; Kolehmainen, E.; Sievänen, E.; Toušek, J. *Curr. Org. Chem.* **2007**, *11*, 1154−1205.
(40) Still, B. M.; Kumar, A.; Aldrich-Wright, J. R.; Price, W. S. *Chem. Soc. Rev.* **2007**, *36*, 665−686.
(41) Bodenhausen, G.; Ruben, D. J. *Chem. Phys. Lett.* **1980**, *69*, 185−189.
(42) Davis, A. L.; Keeler, J.; Laue, E. D.; Moskau, D. *J. Magn. Reson.* **1992**, *98*, 207−216.
(43) Bax, A.; Summers, M. F. *J. Am. Chem. Soc.* **1986**, *108*, 2093−2094.
(44) Willker, W.; Leibfritz, D.; Kerssebaum, R.; Bermel, W. *Magn. Reson. Chem.* **1993**, *31*, 287−292.
(45) Marek, R.; Králík, L.; Sklenář, V. *Tetrahedron Lett.* **1997**, *38*, 665−668.
(46) Maliňáková, K.; Novosadová, L.; Lahtinen, M.; Kolehmainen, E.; Brus, J.; Marek, R. *J. Phys. Chem. A* **2010**, *114*, 1985−1995.
(47) Maliňáková, K.; Novosadová, L.; Pipíška, M.; Marek, R. *ChemPhysChem* **2011**, *12*, 379−388.
(48) Burla, M. C.; Camalli, M.; Carrozzini, B.; Cascarano, G.; Giacovazzo, C.; Polidori, G.; Spagna, R. *Acta Crystallogr.* **2000**, *A56*, 451−457.
(49) Sheldrick, G. M. *Acta Crystallogr., Sect. A* **2008**, *A64*, 112−122.
(50) Becke, A. D. *J. Chem. Phys.* **1993**, *98*, 5648−5652.
(51) Becke, A. D. *Phys. Rev. A* **1988**, *38*, 3098−3100.
(52) Hariharan, P. C.; Pople, J. A. *Theor. Chim. Acta* **1973**, *28*, 213−222.
(53) Figgen, D.; Peterson, K. A.; Dolg, M.; Stoll, H. *J. Chem. Phys.* **2009**, *130*, 164108.
(54) Frisch, M. J.; Trucks, G. W.; Schlegel, H. B.; Scuseria, G. E.; Robb, M. A.; Cheeseman, J. R.; Montgomery, J. A.; Jr., Vreven, T.; Kudin, K. N.; Burant, J. C.; Millam, J. M.; Iyengar, S. S.; Tomasi, J.; Barone, V.; Mennucci, B.; Cossi, M.; Scalmani, G.; Rega, N.; Petersson, G. A.; Nakatsuji, H.; Hada, M.; Ehara, M.; Toyota, K.; Fukuda, R.; Hasegawa, J.; Ishida, M.; Nakajima, T.; Honda, Y.; Kitao, O.; Nakai, H.; Klene, M.; Li, X.; Knox, J. E.; Hratchian, H. P.; Cross, J. B.; Bakken, V.; Adamo, C.; Jaramillo, J.; Gomperts, R.; Stratmann, R. E.; Yazyev, O.; Austin, A. J.; Cammi, R.; Pomelli, C.; Ochterski, J. W.; Ayala, P. Y.; Morokuma, K.; Voth, G. A.; Salvador, P.; Dannenberg, J. J.; Zakrzewski, V. G.; Dapprich, S.; Daniels, A. D.; Strain, M. C.; Farkas, O.; Malick, D. K.; Rabuck, A. D.; Raghavachari, K.; Foresman, J. B.; Ortiz, J. V.; Cui, Q.; Baboul, A. G.; Clifford, S.; Cioslowski, J.; Stefanov, B. B.; Liu, G.; Liashenko, A.; Piskorz, P.; Komaromi, I.; Martin, R. L.; Fox, D. J.; Keith, T.; M. A. Al-Laham., Peng, C. Y.; Nanayakkara, A.; Challacombe, M.; Gill, P. M. W.; Johnson, B.; Chen, W.; Wong, M. W.; Gonzalez, C.; Pople, J. A. *Gaussian 03*, Revision D.01; Gaussian, Inc.: Wallingford, CT, 2004.
(55) (a) Wolinski, K.; Hinton, J. F.; Pulay, P. *J. Am. Chem. Soc.* **1990**, *112*, 8251−8260. (b) Helgaker, T.; Jørgensen, P. *J. Chem. Phys.* **1991**, *95*, 2595−2601.
(56) Standara, S.; Malináková, K.; Marek, R.; Marek, J.; Hocek, M.; Vaara, J.; Straka, M. *Phys. Chem. Chem. Phys.* **2010**, *12*, 5126−5139.
(57) Pawlak, T.; Munzarová, M. L.; Pazderski, L.; Marek, R. *J. Chem. Theory Comp.* **2011**, *7*, 3909−3923.
(58) Miertuš, S.; Scrocco, E.; Tomasi, J. *Chem. Phys.* **1981**, *55*, 117−129.
(59) Tomasi, J.; Mennucci, B.; Cammi, R. *Chem. Rev.* **2005**, *105*, 2999−3093.
(60) Gilbert, T. M.; Ziegler, T. *J. Phys. Chem. A* **1999**, *103*, 7535−7543.
(61) Wodrich, M. D.; Corminboeuf, C. *J. Phys. Chem. A* **2009**, *113*, 3285−3290.
(62) Baerends, E. J.; Autschbach, J.; Bashford, D.; A. Bérces., Bickelhaupt, F.M.; Bo, C.; Boerrigter, P. M.; Cavallo, L.; Chong, D. P.; Deng, L.; Dickson, R. M.; Ellis, D. E.; M. van Faassen., Fan, L.; Fischer, T. H.; C. Fonseca Guerra., Ghysels, A.; Giammona, A.; S. J. A. van Gisbergen., A. W. Götz., Groeneveld, J. A.; Gritsenko, O. V.; M. Grüning., Harris, F. E.; P. van den Hoek., Jacob, C. R.; Jacobsen, H.; Jensen, L.; G. van Kessel., Kootstra, F.; Krykunov, M. V.;

E. van Lenthe., McCormack, D. A.; Michalak, A.; Mitoraj, M.; Neugebauer, J.; Nicu, V. P.; Noodleman, L.; Osinga, V. P.; Patchkovskii, S.; Philipsen, P. H. T.; Post, D.; Pye, C. C.; Ravenek, W.; J. I. Rodríguez., Ros, P.; Schipper, P. R. T.; Schreckenbach, G.; Seth, M.; Snijders, J. G.; M. Solà., Swart, M.; Swerhone, D.; G. te Velde., Vernooijs, P.; Versluis, L.; Visscher, L.; Visser, O.; Wang, F.; Wesolowski, T. A.; E. M. van Wezenbeek., Wiesenekker, G.; Wolff, S. K.; Woo, T. K.; Yakovlev, A. L.; Ziegler, T. *ADF2009.01*; SCM: Amsterdam, The Netherlands, 2009.

(63) Klamt, A. *J. Phys. Chem.* **1995**, *99*, 2224−2235.

(64) Sečkářová, P.; Marek, R.; Malináková, K.; Kolehmainen, E.; Hocková, D.; Hocek, M.; Sklenář, V. *Tetrahedron Lett.* **2004**, *45*, 6259−6263.

(65) Bartl, T.; Zacharová, Z.; Sečkářová, P.; Kolehmainen, E.; Marek, R. *Eur. J. Org. Chem.* **2009**, 1377−1383.

(66) Marek, R.; Křístková, A.; Maliňáková, K.; Toušek, J.; Marek, J.; Hocek, M.; Malkina, O. L.; Malkin, V. G. *J. Phys. Chem. A* **2010**, *114*, 6689−6700.

(67) Bondi, A. *J. Phys. Chem.* **1964**, *68*, 441−451.

(68) García-Raso, A.; Fiol, J. J.; Albertí, F. M.; Lagos, Y.; Torres, M.; Barceló-Oliver, M.; Prieto, M. J.; Moreno, V.; Mata, I.; Molins, E.; Estarellas, C.; Frontera, A.; Quiñonero, D.; Deyà, P. M. *Eur. J. Inorg. Chem.* **2010**, 5617−5628.

(69) Trávníček, Z.; Matiková-Malarová, M.; Novotná, R.; Vančo, J.; Štěpánková, K.; Suchý, P. *J. Inorg. Biochem.* **2011**, *105*, 937−948.

(70) Pyykkö, P. *Chem. Phys.* **1983**, *74*, 1−7.

(71) Malkin, V. G.; Malkina, O. L.; Salahub, D. R. *Chem. Phys. Lett.* **1996**, *261*, 335−345.

(72) Kaupp, M.; Malkina, O. L.; Malkin, V. G.; Pyykkö, P. *Chem.—Eur. J.* **1998**, *4*, 118−126.

(73) Vaara, J.; Manninen, P.; Lantto, P. In *Calculation of NMR and EPR Parameters: Theory and Applications*; Kaupp, M., Buhl, M., Malkin, V. G. Wiley-VCH: Weinheim, Germany,2004; pp 209−226.